New Journal of Physics
The open access journal at the forefront of physics

Deutsche Physikalische Gesellschaft DPG
IOP Institute of Physics

Published in partnership with: Deutsche Physikalische Gesellschaft and the Institute of Physics

OPEN ACCESS

RECEIVED
30 June 2020

REVISED
4 August 2020

ACCEPTED FOR PUBLICATION
10 August 2020

PUBLISHED
9 September 2020

PAPER

Trade-off between filtering and symmetry breaking mean-field coupling in inducing macroscopic dynamical states

Uday Singh[1], K Sathiyadevi[2], V K Chandrasekar[3], W Zou[4], J Kurths[5,6,7] and D V Senthilkumar[1]

[1] School of Physics, Indian Institute of Science Education and Research, Thiruvananthapuram-695551, India
[2] Centre for Nonlinear Dynamics, School of Physics, Bharathidasan University, Tiruchirappalli-620024, Tamil Nadu, India
[3] Centre for Nonlinear Science and Engineering, School of Electrical and Electronics Engineering, SASTRA Deemed University, Thanjavur-613401, Tamil Nadu, India
[4] School of Mathematical Sciences, South China Normal University, Guangzhou 510631, People's Republic of China
[5] Potsdam Institute for Climate Impact Research, Telegraphenberg, Potsdam D-14415, Germany
[6] Institute of Physics, Humboldt University Berlin, Berlin D-12489, Germany
[7] Saratov State University, 83, Astrakhanskaya Str., 410012 Saratov, Russia

E-mail: skumar@iisertvm.ac.in

Keywords: symmetry breaking coupling, aging transition, low-pass filter

Abstract

We study the manifestation of the competing interaction between the mean-field intensity and the symmetry breaking coupling on the phenomenon of aging transition in an ensemble of limit-cycle oscillators comprising of active and inactive oscillators. Further, we also introduce filtering in both the intrinsic and extrinsic variables of the mean-field diffusive coupling to investigate the counter-intuitive effect of both filterings. We find that large values of the mean-field intensity near unity favor the oscillatory nature of the ensemble, whereas low values favor the onset of the aging transition and heterogeneous dynamical states such as cluster oscillation death and chimera death states even at low values of the symmetry breaking coupling strength. Heterogeneous dynamical states predominates at large values of the coupling strength in all available parameter spaces. We also uncover that even a weak intrinsic filtering favors the aging transition and heterogeneous dynamical states, while a feeble extrinsic filtering favors the oscillatory state. Chimera death state is observed among the active oscillators for the first time in the aging literature. Our results can lead to engineering the dynamical states as desired by an appropriate choice of the control parameters. Further, the transition from the oscillatory to the aging state occurs via an inverse Hopf bifurcation, while the transition from the aging state to the cluster oscillation death states emerges through a supercritical pitch-fork bifurcation. The deduced analytical bifurcation curves are in good agreement with the numerical boundaries of the observed dynamical states.

1. Introduction

The framework of coupled nonlinear oscillators is a veritable black box facilitating the onset of a plethora of intriguing collective dynamical behaviors mimicking several real-world phenomena such as clustering [1–4], synchronization [1–5], death states [5–10], chimera states [11–13], etc. Coupled nonlinear oscillators have also been used as a key framework to elucidate the nature of life, as their emerging dynamics underlie circadian rhythms, heart contraction, event related synchronization/desynchronization responsible for various cognitive, motor and sensory tasks, peristaltic motion of gastrointestinal tracts, etc cf ([14–18]). The phenomenon of AG was introduced by Diado and Nakanishi [19] in view of understanding the robustness of the self-oscillatory nature of the coupled oscillators and the underlying mechanism for the loss of macroscopic activity due to an increase in the number of non-oscillatory oscillators because of some kind of damages or deterioration similar to the cascading failures in networks and power grids [20]. Originally, AG was reported in an ensemble of globally coupled oscillators by increasing the proportion of

inactive oscillators [19] and later it has been extended to diffusively coupled oscillators [21]. There lies a growing body of evidence on the phenomenon of AG probing the mechanism for the loss of macroscopic oscillations in an ensemble comprising active and inactive oscillators [21–35]. For instance, introducing asymmetry in the dispersal rates found to enhance the meta-population survivability from local extinctions [36].

AG, attributing to the manifestation of a homogeneous steady state among the ensemble of coupled oscillators, has been reported so far only by adopting symmetry coupling [21–31, 33]. The role of symmetry breaking coupling on the onset of the AG in an ensemble comprising active and inactive oscillators is unclear yet. Further, the mean-field coupling is known to facilitate the onset of the homogeneous steady state (amplitude death) in two-coupled oscillators [37, 38], where it was emphasized that '*mean-field coupling is a much stronger* '*trap*' *to induce death compared to other coupling schemes*'. So a next natural question is whether the mean-field coupling can facilitate the onset of the homogeneous steady state in a network of oscillators, comprising active and inactive ones, facilitating the AG? Indeed, the symmetry breaking coupling is known to favor the onset of heterogeneous dynamical states [8, 9, 39]. Now, a more curious question is what would be the manifestation of the competing interaction of the mean-field and the symmetry breaking couplings on the AG? Further, very recent investigations have employed low-pass filters (LPF) to revoke the stability of stable homogenous/inhomogeneous steady states and to revive the oscillations in the same parameter space where the coupled oscillators suffered death (inactive) states [40, 41], thereby increasing the robustness of the self-sustained oscillatory nature including the macroscopic activity of the coupled oscillators. Notably, an LPF was deployed to introduce an additional unstable degree of freedom in order to rule out the odd number limitation in the control theory [42]. In this paper, we introduce the LPF in both variables of the mean-field diffusive coupling and investigate the effect of their cut-off frequencies on the AG in addition to the competing effects of the mean-field and the symmetry breaking couplings.

We consider an ensemble of limit-cycle oscillators with mean-field diffusive coupling breaking the rotational symmetry of the coupled system. We find that the symmetry breaking coupling facilitates the transition from cluster oscillatory state (COS) to the homogeneous state (AG) and then to heterogeneous states, such as cluster oscillation death (COD) and chimera death (CD) states. COS state simply refers to clusters of oscillatory state [43, 44]. AG refers to the loss of macroscopic oscillations, through stabilization of trivial steady state, due to deterioration/failures of local nodes of the network [19]. CD is basically reported as a sandwich of the dynamical nature of the chimera states [45] and the heterogeneous nature of the oscillation death [7, 8]. The CD refers to coexisting coherent and incoherent domains comprising of neighbouring oscillators populating the same branch and different branches, respectively, of the inhomogeneous steady state [9, 46–48]. COD state refers to clusters of oscillation death state [48–50]. Nevertheless, limiting the mean-field interaction using the mean-field intensity parameter favors the onset of the AG, COD and CD states even for low values of the symmetry breaking coupling strength, thereby increasing the spread of these dynamical states in a large range of the coupling strength. Further, the cut-off frequency of the intrinsic variable facilitates the onset of both the stable homogeneous and heterogeneous steady states in a large range of the coupling strength. In contrast, the cut-off frequency of the extrinsic variable facilitates the COS by switching the stability of the stable homogeneous and heterogeneous steady states even in the presence of filtering in the intrinsic variable, which actually favors the stablilization of both the steady states. COS comprising high and low amplitude oscillations corresponding to the active and inactive oscillators, respectively, predominate and prevail for low values of the coupling strength in the entire explored range of the mean-field parameter, intrinsic and extrinsic cut-off frequencies. Bistability among the three different dynamical states is also observed in the system parameter space. We find that the transition from COS to aging transition (AG) is mediated by an inverse Hopf bifurcation (HB), while the transition from AG to COD is facilitated by a supercritical pitch-fork bifurcation (PB). Further, the analytical critical curves corresponding to the HB and PB curves are also deduced for the mean-field symmetry breaking coupling without any filtering. The PB curve is also deduced in the presence of intrinsic and extrinsic filtering in the mean-field diffusive coupling. The analytical critical curves are found to agree perfectly with the simulation results.

The plan of the paper is as follows. The paradigmatic model of the Stuart–Landau limit cycle oscillators with a mean-field symmetry breaking coupling including filtering in both variables of the mean-field diffusive coupling will be discussed in section 2. Dynamical transitions using the normalized global order parameter, one parameter bifurcation diagram obtained using XPPAUT illustrating the effect of the filtering in the coupling, and the manifestation of the competing interaction between the mean-field intensity parameter and symmetry breaking coupling will be detailed in section 3. Global dynamical transitions using various two parameter phase diagrams will be discussed in section 4, and in section 5, we will provide a summary and conclusions.

2. Model

We consider an ensemble of the paradigmatic Stuart–Landau limit-cycle oscillators, which represents the normal form of the HB and hence many nonlinear oscillators exhibiting HB can be approximated as Stuart–Landau oscillator [51–53], with LPF in both the intrinsic and extrinsic variables of the mean-field diffusive coupling, whose governing equation of motion can be expressed as

$$\dot{z}_j = \left(\lambda_j + i\omega - |z_j|^2\right) z_j + \varepsilon\left(Qu - v_j\right), \tag{1a}$$

$$\dot{v}_j = \alpha\left(-v_j + \mathrm{Re}(z_j)\right), \tag{1b}$$

$$\dot{u} = \beta\left(-u + \frac{1}{N}\sum_{k=1}^{N}\mathrm{Re}(z_j)\right), \tag{1c}$$

where $z_j = r\ \mathrm{e}^{\mathrm{i}\theta_j} = x_j + iy_j \in C$, $j = 1, \ldots, N$. x_j and y_j are the state variables of the system. λ_j is the Hopf-bifurcation parameter with limit cycle oscillations for $\lambda_j > 0$ and a stable trivial steady state for $\lambda_j < 0$. The active oscillators with limit cycle oscillations are assigned $\lambda_j = 2$, while those for the inactive oscillators are chosen as $\lambda_j = -1$. The active oscillators are indexed as $j \in 1, \ldots, N(1-p)$, while those of the inactive oscillators are $j \in N(1-p)+1, \ldots, N$, where the parameter p corresponds to the proportion of the inactive oscillators. All the oscillators are active when $p = 0$, whereas all the oscillators are inactive for $p = 1$. Intermediate values of $0 < p < 1$ determine the proportion of active and inactive oscillators in the ensemble. ω is the natural frequency of the oscillation, ε is the coupling strength, the mean-field intensity parameter Q determines the degree of the mean-field interaction. $Q = 1$ quantifies the maximum mean-field interaction, whereas $Q < 1$ corresponds to a limited mean-field interaction, which results in a plethora of nontrivial intriguing dynamical states. For instance, Q controls the additional mortality in the meta-population dynamics in ecology during their dispersal [54], Q is a quorum sensing parameter in the context of the synthetic genetic oscillators controlling the degree of dilution [55–57]. The mean-field extrinsic variable $u(t)$ and the intrinsic variable $v_j(t)$ in the coupling are governed by the linear ordinary differential equations for LPFs related to z_j as in equations (2b) and (2c), respectively. LPF disperse and attenuates the high frequency signals thereby filtering them and their harmonics, and passing only the low frequency components. The cutoff frequencies α and β determine the degree of attenuation of the intrinsic and extrinsic signals, respectively. In the limit of $\alpha \to \infty$, $v_j = \mathrm{Re}(z_j)$ and in the limit of $\beta \to \infty$, $u = \sum_j \frac{\mathrm{Re}(z_j)}{N}$ and hence the coupling in equation (1) reduces to the standard mean-field diffusive coupling. Attenuation of the intrinsic and extrinsic signals will be stronger for relatively smaller α and β as the higher frequencies and their harmonics are filtered out. In contrast, higher values of α and β correspond to a relatively weak filtering. The mean-field coupling employed only in the x_j variable explicitly breaks the rotational symmetry of the coupled Stuart–Landau limit cycle oscillators thereby loosing the rotational invariance under the transformation $z_j \to z_j \mathrm{e}^{i\theta}$.

3. Dynamical transitions

3.1. Dynamical transitions using order parameter

To elucidate the dynamical transitions as a function of the proportion of inactive oscillators p, the normalized global order parameter $K \equiv |Z(p)|/|Z(0)|$ is depicted in figures 1(a) and (b) for three different values of the intrinsic and extrinsic cut-off frequencies α and β, respectively. The order parameter $Z = 1/N\sum_{j=1}^{N} z_j$, while $Z(p)$ and $Z(0)$ are the order parameters for $0 < p \leqslant 1$ and $p = 0$, respectively. $K = 0$ corroborates the onset of the AG. The total number of oscillators and the natural frequency of the oscillation are fixed as $N = 100$ and $\omega = 3.0$ throughout the manuscript. The coupling strength is fixed as $\varepsilon = 6.0$ in figure 1. We find that the normalized order parameter $K \to 0$ as $p \to 1$ and saturates at $K = 0$ only when $p = 1$ as depicted in figure 1(a) for $\alpha = 3.0$ and $\beta = 8.0$. However, the AG occurs at $p_c = 0.79$ for $\alpha = 5.0$ [see figure 1(a)] elucidating that the intrinsic cut-off frequency (weak intrinsic filtering) indeed facilitates the onset of the AG even in the presence of a finite proportion of the active oscillators. It is also evident from the figure that K saturates at the null value at $p_c = 0.36$ for $\alpha = 8.0$ strongly corroborating that even a weak intrinsic filtering favors the onset of the AG despite the presence of a large proportion of active oscillators.

In contrast, relatively weak filtering of the extrinsic variable favors the oscillatory state by destabilizing the stable homogeneous steady state, that is the AG, of the ensemble of the limit-cycle oscillators. The normalized order parameter K is depicted in figure 1(b) for three different β and $\alpha = 5.0$. The AG occurs at $p_c = 0.52$ for $\beta = 4.0$. Upon increasing the cut-off frequency further, K acquires the null value only at

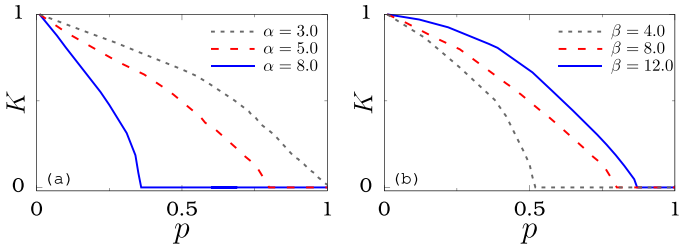

Figure 1. Normalized global order parameter K as a function of the inactive ratio p of system (1) for (a) $\alpha = 3.0, 5.0$ and $\alpha = 8.0$, and $\beta = 8.0$, and (b) $\beta = 4.0, 8.0$ and $\beta = 12.0$, and $\alpha = 5.0$. Other parameters: $a = 2.0$, $b = -1.0$, $\omega = 3.0$, $Q = 0.5$, $\varepsilon = 6.0$ and $N = 100$. Normalized global order parameter K is plotted to idenfify the dynamical phase transitions. K attains null value at $p = p_c$ elucidating onset of the AG, that is, loss of macroscopic oscillatory state. The network exhibits macroscopic oscillations for $p < p_c$ and remains at the stable homogeneous trivial steady state, representing AG, for $p > p_c$.

$p_c = 0.8$ for $\beta = 8.0$ elucidating that the AG occurs for a rather higher value of $p \geqslant 0.8$. This implies that large values of β (weak extrinsic filtering) favor the oscillatory state even in the presence of a large proportion of inactive oscillators thereby increasing the robustness of the network and preserving the macroscopic activity. For $\beta = 12.0$, the oscillatory state prevails in the range of $p \in (0, 0.88)$ beyond which the network of oscillators suffers the AG [see figure 1(b)]. Thus, it is evident that even a weak intrinsic filtering favors the onset of the AG despite the presence of a large proportion of active oscillators, while the weak extrinsic filtering favors the oscillatory state despite the presence of a large fraction of inactive oscillators and intrinsic filtering, which actually favor the stable steady state. It is also to be noted that the inverse effect is also true for strong filtering, that is, strong intrinsic (extrinsic) filtering facilitates oscillatory (aging) state [see figures 1(a) and (b)].

3.2. Dynamical transitions using one-parameter bifurcation diagram

To analyse the dynamical transitions using one-parameter bifurcation diagrams and to find the stable boundaries of the observed dynamical states as a function of the system parameters, equation (1) can be reduced in terms of active ($z_j = z_A$) and inactive ($z_j = z_I$) oscillators as

$$\begin{aligned}
\dot{z}_A &= (2 + i\omega - |z_A|^2)z_A + \varepsilon(Qu - v_A),\\
\dot{v}_A &= \alpha(-v_A + \mathrm{Re}(z_A)),\\
\dot{z}_I &= (-1 + i\omega - |z_I|^2)z_I + \varepsilon(Qu - v_I),\\
\dot{v}_I &= \alpha(-v_I + \mathrm{Re}(z_I)),\\
\dot{u} &= \beta(-u + p\ \mathrm{Re}(z_I) + (1-p)\mathrm{Re}(z_A)),
\end{aligned} \tag{2}$$

where $z_A = x_A + iy_A$ and $z_I = x_I + iy_I$.

One parameter bifurcation diagrams, obtained using XPPAUT, of the above reduced equation are shown in figure 2 for $p = 0.8$ as a function of the coupling strength displaying the effect of the intrinsic and extrinsic cut-off frequencies α and β on the AG region. The COS, comprising a large (indicated by filled squares) and a small (indicated by filled triangles) amplitude limit-cycle oscillations of active and inactive oscillators, respectively, is observed in the range of $\varepsilon \in (2, 5.13]$ [see figure 2(a) plotted for $\alpha = 5.0$ and $\beta = 4.0$]. Stabilization of the trivial fixed point of all the oscillators in the ensemble occurs through an inverse HB at $\varepsilon = 5.14$ manifesting the onset of the AG in the range of $\varepsilon \in [5.14, 7.39)$ (shaded region). A large strength of the symmetry breaking coupling favors the heterogeneous dynamical states. A COD state onsets via a PB at $\varepsilon = 7.39$ and prevails in the entire higher values of ε. Similar dynamical transitions are observed in figures 2(b) and (c) for different sets of α and β but illustrating the effect of the intrinsic and extrinsic cut-off frequencies on the AG region. Increasing β, from 4.0 in figure 2(a) to 8.0 in figure 2(b), for the same $\alpha = 5.0$ increases the COS state in the range $\varepsilon \in (2, 5.9]$ thereby decreasing the spread of the AG state in the further narrow range of $\varepsilon \in (5.9, 7.39)$. This corroborates that the weak extrinsic filtering destabilizes the stable trivial steady state of all the oscillators thereby facilitating the re-emergence of the oscillatory state in the same parameter space where the network suffered the AG. Now by fixing the extrinsic cut-off frequency at $\beta = 8.0$ as in figure 2(b) and increasing the intrinsic cut-off frequency from $\alpha = 5.0$ to $\alpha = 8.0$, the spread of the AG state (shaded region) is enhanced to a larger range of $\varepsilon \in (4.34, 7.39)$ [see figure 2(c)] corroborating that a weak intrinsic filtering favors the aging state.

To appreciate the dynamical nature of the COS, AG and COD states, their spatio-temporal plots (first column) and time traces (second column) are depicted in figure 3 for the same parameters as in figure 2(a).

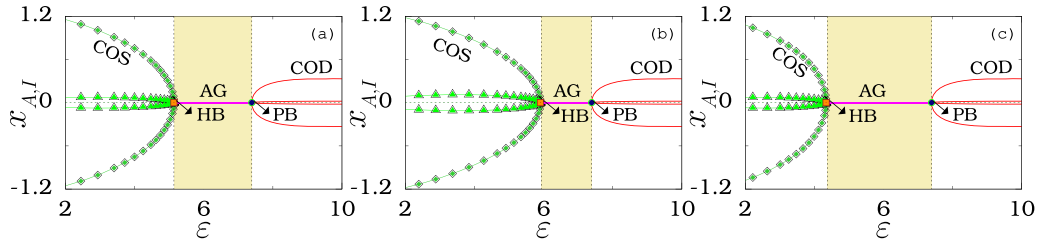

Figure 2. One parameter bifurcation diagram (using XPPAUT) as a function of the coupling strength (ε) of system (2) for (a) $\alpha = 5.0$, $\beta = 4.0$, (b) $\alpha = 5.0$, $\beta = 8.0$, and (c) $\alpha = 8.0$. $\beta = 8.0$. HB and PB are the HB and PB points. COS, AG and COD represent the cluster oscillatory, aging and COD states, respectively. Other parameters: $a = 2.0$, $b = -1.0$, $\omega = 3.0$, $Q = 0.5$, and $p = 0.8$. It is depicted to understand the dynamical transitions among different observed dynamical states. The figure elucidates that weak extrinsic filtering destabilizes the stable trivial steady state thereby facilitating the re-emergene of the oscillatory state in the same parameter space where the network suffered the AG. It also reveals that a weak intrinsic filtering favors the aging state.

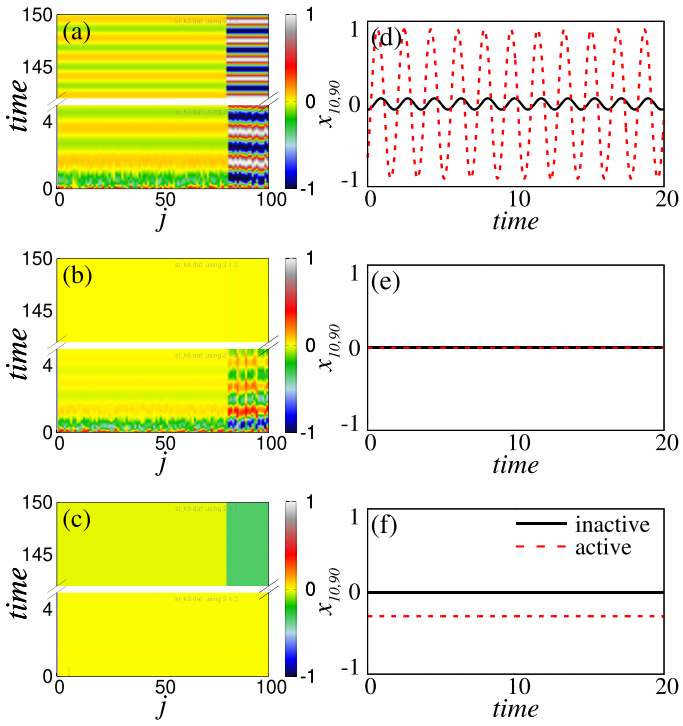

Figure 3. In order to appreciate the dynamical nature of the COS, aging and COD states observed in the one parameter bifurcation digram, figure 2, spatio-temporal and time evolutions of system (2) for (a) and (d) COS ($\varepsilon = 3.0$), (b) and (e) aging state ($\varepsilon = 6.0$), and (c) and (f) COD state ($\varepsilon = 9.0$) are depicted. Other parameters are the same as in figure 2(a). The nature of initial conditions employed can be recognised by the color coding from the early states of the evolution of the depicted dynamical states. See text for more details.

The time evolution of the representative oscillators from the inactive group (x_{10}) and the active group (x_{90}) are depicted in the second column. The COS comprising large and small oscillations of the active and inactive oscillators is shown in figures 3(a) and (d) for $\varepsilon = 3.0$. The AG is displayed in figures 3(b) and (e) for $\varepsilon = 6.0$, where the trivial steady state of the active and inactive oscillators is stabilized resulting in the manifestation of the stable homogeneous steady state. The COD state is depicted in figures 3(c) and (f) for $\varepsilon = 9.0$, where the inactive oscillators populate the stable homogeneous steady state, while the active oscillators populate one of the branches of the inhomogeneous steady states depending on the distribution of their initial states. Random initial conditions are chosen for COS and AG states, while cluster initial conditions are used for the COD state. Random initial conditions for large values of the symmetry breaking coupling results in the manifestation of the CD state among the active oscillators, which will be discussed later.

3.2.1. Trade-off between the mean-field and symmetry breaking couplings

Now, we will discuss the effect of the competing interaction only between the mean-field intensity Q and the strength of the symmetry breaking coupling ε on the AG in the absence of both the intrinsic and

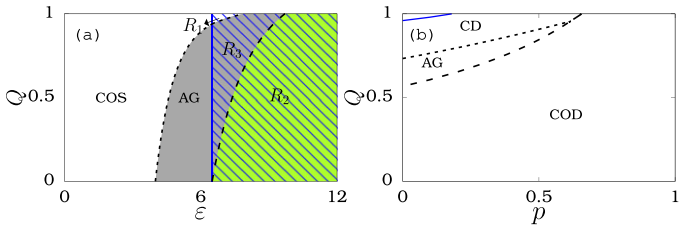

Figure 4. Dynamical transitions elucidating the competing interaction between the mean-field intensity parameter Q, and the symmetry breaking coupling without any filtering in the extrinsic and intrinsic variables (a) in the (ε, Q) parameter space for $p = 0.8$ and (b) in the (p, Q) parameter space for $\varepsilon \in (0, 12)$. This figure elucidates that the mean-field intensity parameter Q favors both the homogeneous steady state (AG) and heterogeneous symmetry breaking states (COD) in the appropriate ranges of the symmetry breaking coupling strength ε and the fraction of inactive oscillators p.

extrinsic filtering in the coupling. The observed dynamical transition is shown in figure 4 as a two phase diagram in the (ε, Q) parameter space. We identify a transition from the COS (unshaded region) to the COD (green/light grey region) state via the AG (dark grey region) as a function of ε in the entire range of Q. Nevertheless, there is a bistability between the CD state and COS, COD, and AG states (in the two parameter space shaded with diagonal lines) in the R_1, R_2 and R_3 regions, respectively. A COS is observed near the unit value of the mean-field intensity parameter Q in a large range of ε, whereas AG and COD states are observed in a rather narrow range of ε. Interestingly, decreasing Q, that is limiting the mean-field interaction, results in an increase in the spread of AG and COD states as a function of ε [see figure 4(a)] elucidating that the mean-field intensity parameter favors both the homogeneous steady state (AG) and heterogeneous symmetry breaking states (COD) in the appropriate ranges of the symmetry breaking coupling. It is also to be noted that the onset of AG and COD occurs even for low values of ε upon decreasing the mean-field intensity parameter. Further, a large value of the symmetry breaking coupling induces symmetry breaking states in the entire range of Q. The homogeneous steady state (AG) is always found to be preceded by the COS, while the heterogeneous symmetry breaking states (COD) by the homogeneous steady state (AG region). The transition from COS to AG is mediated by an inverse HB, while that from AG to COD is by a PB. The parameter space of the CD state is independent of the mean field intensity Q.

The HB and PB curves can be deduced from equation (2). As there is no filtering in the coupling, equation (2) can be further reduced as

$$\dot{z}_{\rm A} = (2 + i\omega - |z_{\rm A}|^2)z_{\rm A} + \varepsilon(Qu - {\rm Re}(z_{\rm A})), \tag{3a}$$

$$\dot{z}_{\rm I} = (-1 + i\omega - |z_{\rm I}|^2)z_{\rm I} + \varepsilon(Qu - {\rm Re}(z_{\rm I}), \tag{3b}$$

where $u = p{\rm Re}(z_{\rm I}) + (1-p){\rm Re}(z_{\rm A})$. The corresponding characteristic equation can be written as

$$\lambda^4 + A_3\lambda^3 + A_2\lambda^2 + A_1\lambda + A_0 = 0. \tag{4}$$

The coefficients A_0, A_1, A_2, and A_3 can be expressed as

$$\begin{aligned}
A_0 &= (a^2+\omega^2)(b^2+\omega^2+b\varepsilon(1-pQ)) - a\varepsilon(b^2+\omega^2)(1+\hat{p}Q) - b\varepsilon Q_1,\\
A_1 &= b^2\varepsilon(1+\hat{p}Q) - Q_2\omega^2\varepsilon + a^2\left(2b + \varepsilon(1-pQ) + b(2\omega^2 - Q_1\varepsilon^2) + a(Q_1\varepsilon^2 + 2bQ_2\varepsilon - 2(b^2+w^2)\right),\\
A_2 &= a^2 + b^2 + 2\omega^2 + b(3 + (p-2)Q)\varepsilon - \varepsilon^2 Q_1 + a((Q(1+P) - 3)\varepsilon - 4b),\\
A_3 &= 2(b-a) - Q_2\varepsilon,
\end{aligned} \tag{5}$$

where $\hat{p} = p - 1$, $Q_1 = Q - 1$ and $Q_2 = Q - 2$. The critical curve, the HB curve, separating AG and COD can be obtained from $A_0 = 0$ as

$$Q_{\rm c} = \frac{(a^2+\omega^2-a\varepsilon)(b^2+\omega^2+b\varepsilon)}{\varepsilon(a\hat{p}(b^2+\omega^2-b\varepsilon) + bp(a^2+\omega^2))}. \tag{6}$$

The HB curve separating COS to AG can be deduced from the condition,

$$\frac{(A_1^2 - A_1A_2A_3 + A_0A_3^2)}{(A_1 - A_2A_3)} > 0. \tag{7}$$

The corresponding analytical Hopf (dotted line) and pitch-fork (dashed line) bifurcation curves are depicted in figure 4(a), which agree very well with the numerical boundaries.

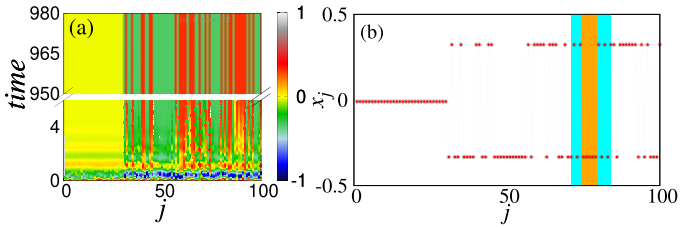

Figure 5. To appreciate the CD state observed in the two parameter phase diagram in figure 4(b) (a) spatio-temporal and (b) snap-shot of CD state for $\varepsilon = 9.0, p = 0.3$ and $Q = 0.5$ are depicted here. Representative incoherent (cyan/light grey) and coherent (orange/dark grey) domains are shaded in figure 5(b).

For a further insight into the observed dynamical states, the spread of the COS, AG, COD, and CD states is depicted in figure 4(b) in the (p, Q) parameter space for $\varepsilon \in (0, 15)$. The spread of the dynamical states as a function of ε is obtained for a fixed Q and p, which has to be repeated as a function of p. This procedure results in a set of spread for each COS, AG and COD states as a function of p for a fixed Q for different values of ε in the range of $\varepsilon \in (0, 15)$. The superimposed spreads of each dynamical state in the range of $\varepsilon \in (0, 12)$ are obtained as a function of p for a fixed Q, which is repeated again as a function Q. Now, we get a global picture of the spread of the observed dynamical states in the explored range of p, Q and ε in the two-parameter phase (p, Q) space as depicted in figure 4(b). The COS state is observed in the entire explored range of p and Q for various ε. Similarly, the AG is observed in the entire parameter space below the dotted line, while the COD state is observed in the parameter space below the dashed line. The CD state is observed in the parameter space below the continuous line. For any particular choice of ε, the spread of the observed dynamical states will lie only within their maximum spread depicted in figure 4(b) as a function of p and Q.

The CD state observed among the active oscillators for random initial states of the active and inactive oscillators, comprising the ensemble of Stuart–Landau limit cycle oscillators, is depicted in the spatio-temporal and snap-shot plots in figure 5 for $p = 0.4$. Subsequent active oscillators populating the upper and lower branches alternately constitute the incoherent domain, while the two or more subsequent active oscillators populating either the upper or lower branches constitute the coherent domain of the CD states. Representative coherent and incoherent domains are shaded in figure 5(b).

The submanifold equation for the CD state can be expressed as,

$$\begin{aligned} \dot{z}^{\mathrm{a}}_{1,2} &= (a + i\omega - |z^{\mathrm{a}}_{1,2}|^2) z^{\mathrm{a}}_{1,2} + \varepsilon(u - v_{1,2}), \\ \dot{z}^{\mathrm{i}}_{3} &= (-b + i\omega - |z^{\mathrm{i}}_{3}|^2) z^{\mathrm{i}}_{3} + \varepsilon(u - v_{3}), \\ \dot{v}_{1,2,3} &= \alpha(-v_{1,2,3} + \mathrm{Re}(z_{1,2,3})), \\ \dot{u} &= \beta(-u + \Delta), \end{aligned} \tag{8}$$

where $\Delta = (1/2)(1 - p)\mathrm{Re}(z^{\mathrm{a}}_1 + z^{\mathrm{a}}_2) + p\ \mathrm{Re}(z^{\mathrm{i}}_3)$. z^{a}_1 and z^{a}_2 represent the active group of oscillators, while z^{i}_3 denotes the inactive group of oscillators.

Under the conditions, $z^{\mathrm{in}}_j = 0, \sum_{j=1}^{N} z^{\mathrm{act}}_j = 0$ and $z^{\mathrm{act}}_j \neq 0$, the submanifold equation for the CD state can be reduced as

$$\dot{z}^{\mathrm{act}}_j = (a + i\omega - |z^{\mathrm{act}}_j|^2) z^{\mathrm{act}}_j + \varepsilon \mathrm{Re}\, z^{\mathrm{act}}_j, \tag{9}$$

whose fixed point solution is

$$\begin{aligned} x^* &= \mp \frac{1}{\sqrt{2\varepsilon}} \sqrt{2\omega^2 + \varepsilon(a - \varepsilon) + \sqrt{\varepsilon^2 - 4\omega^2}(\varepsilon - a)}, \\ y^* &= \pm \frac{\varepsilon + \sqrt{\varepsilon^2 - 4\omega^2}}{2\omega} x^*. \end{aligned} \tag{10}$$

These fixed points correspond to the upper and lower branches of the inhomogeneous steady states comprising the coherent and incoherent domains of the CD state depicted in figure 5.

4. Global dynamical transitions

For a global perspective on the effect of all the parameters on the observed dynamical states, and in particular, to appreciate the effect of the intrinsic and extrinsic cut-off frequencies of the filtering, we have

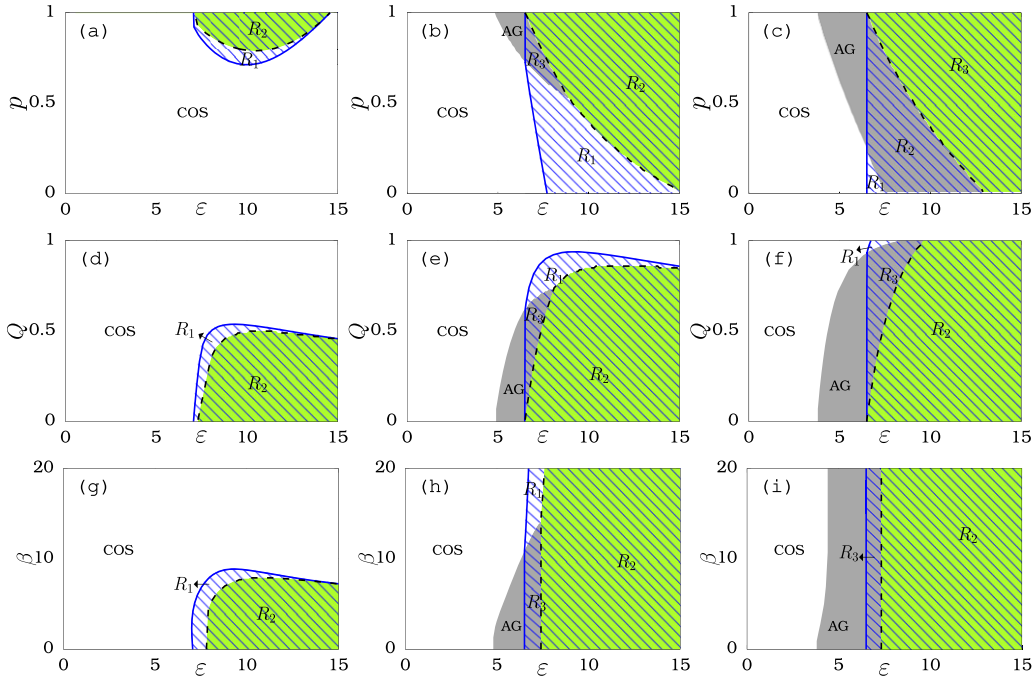

Figure 6. Dynamical transitions in coupled Stuart–Landau limit-cycle oscillators in (a)–(c) (ε, p) space for $\beta = 8.0$ and $Q = 0.5$, (d)–(f) (ε, Q) space for $p = 0.8$ and $\beta = 8.0$, and (g)–(i) (ε, β) space for $p = 0.8$ and $Q = 0.5$ and for the intrinsic cut-off frequency $\alpha = 3.0, 5.0$ and 8.0. Other parameters: $a = 2.0$, $b = -1.0$, $\omega = 3.0$, and $N = 100$. This figure is depicted to elucidate the effect of intrinsic filtering on the observed dynamical states and their spread in various system parameter space. It is evident from the figure that weak intrinsic filtering destabilize both the stable oscillatory state (COS) facilitating the spread of AG state in a large range of the parameter space. It also favors the the spread of heterogeneous symmetry breaking states (COD and CD).

depicted two-parameter phase diagrams in the various parameter spaces in figure 6. It is evident that COS occupies the entire unshaded region. The solid curve encloses the CD state (region shaded with diagonal lines), whereas the dashed curve encloses the COD state (green/light grey region). The dark grey shaded region corresponds to the AG region. Bistability between the COS and CD state is observed in the region R_1, that between CD and COD in the region R_2, and that between CD and AG in the region R_3. The first row (figures 6(a)–(c)) is depicted in the (ε, p) parameter space for three different values of the intrinsic cut-off frequency α for $\beta = 8.0$ and $Q = 0.5$. The coupled Stuart–Landau limit-cycle oscillators do not exhibit the AG for $\alpha = 3.0$ [see figure 6(a)], but the COS state in most of the parameter space. Nevertheless the bistable regions R_1 and R_2 emerge in a small region of the (ε, p) parameter space. Upon increasing the intrinsic cut-off frequency to $\alpha = 5.0$, the AG region appears in a finite region of the parameter space, while the spread of the bistable regions R_1 and R_2 increases to a large extent. Because of the emergence of the AG region, there exists bistability between AG and CD in R_3. Further increase in α to $\alpha = 8.0$, facilitates the spread of the AG to a large extent with an increase in the bistable region R_3 at the cost of R_1 decreasing the spread of the COS state. Similar dynamical transitions are shown in figures 6(d)–(f)(middle row) but in the (ε, Q) parameter space for $\beta = 8.0$ and $p = 0.8$ for the same three values of α as in figures 6(a)–(c). It is also evident from these figures that increasing the values of the intrinsic cut-off frequency facilitate the onset and the spread of the AG region to a large parameter space. Further, a similar effect of α is also evident in the (ε, β) parameter space in figures 6(g) and (h) for $Q = 0.5$ and $p = 0.8$. Thus increasingly weak filtering of the intrinsic variable, in general, facilitates the onset of the AG even at lower values of the coupling strength and the spread of the same to a large region of the available parameter space. Furthermore, it also facilitates the spread of the heterogeneous symmetry breaking states (COD and CD states) in the entire range of the parameters p, Q and β for a large symmetry breaking coupling strength as evident from figure 6.

As in figure 4(a), the dynamical transition from COS to AG occurs through an inverse HB, while the transition from the AG to COD state occurs via a PB. One can also deduce the HB and PB curves, in principle, in the presence of the intrinsic and extrinsic filtering. However, one has to solve a seventh order polynomial equation in λ with a large expression for their coefficients resulting from the Jacobain of a seven by seven matrix corresponding to equation (2), which results in more than two page expressions for the inverse HB curve. Hence, the expression for the latter was not included here. However, one can deduce a simple expression corresponding to the PB curve facilitating the transition from the AG to the COD state,

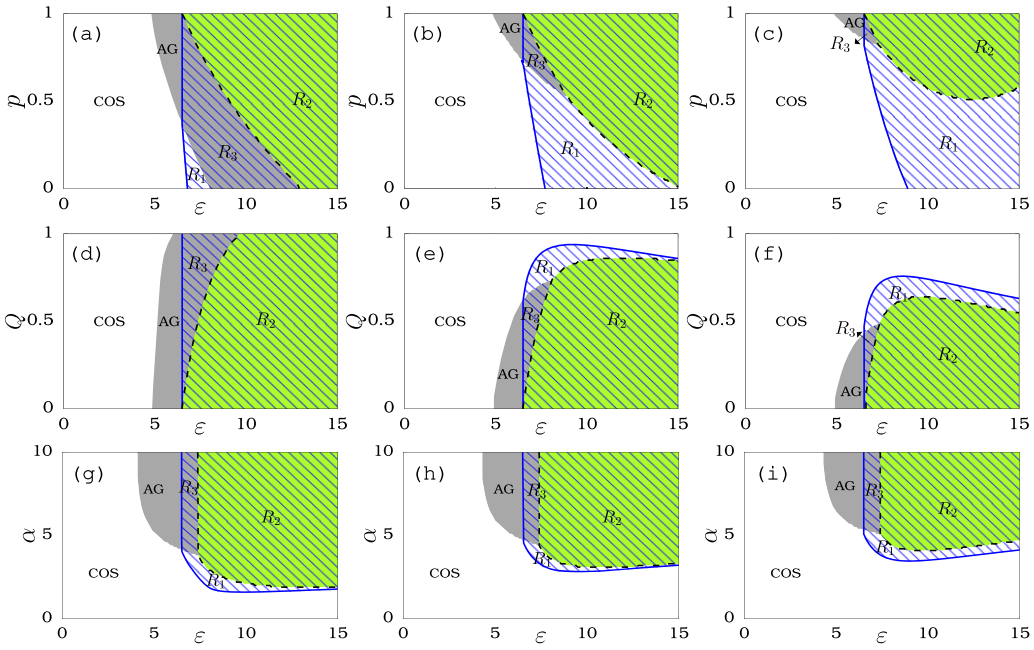

Figure 7. Dynamical transitions in coupled Stuart–Landau limit-cycle oscillators in (a)–(c) (ε, p) space for $\alpha = 5.0$ and $Q = 0.5$, (d)–(f) (ε, Q) space for $p = 0.8$ and $\alpha = 5.0$, and (g)–(i) (ε, α) space for $p = 0.8$ and $Q = 0.5$ for increasing values of the extrinsic cut-off frequency $\beta = 4.0, 8.0$ and 12.0. Other parameters: $a = 2.0$, $b = -1.0$, $\omega = 3.0$, and $N = 100$. This figure is depicted to elucidate the effect of extrinsic filtering on the observed dynamical states and their spread in various system parameter space. It is evident from the figure that weak extrinsic filtering destabilize both the stable homogeneous steady state (AG) and heterogeneous stable symmetry breaking states (COD) state to retain sustained oscillations in a large range of the parameter space.

which can be expressed as

$$p_c = \frac{(b^2 + \omega^2 + b\varepsilon)(a^2 + \omega^2 + a(Q-1)\varepsilon)}{(a+b)Q(ab + \omega^2)\varepsilon}. \tag{11}$$

We have also confirmed that the analytical boundaries match very well with the simulation results in figures 6 and 7.

Now, we will investigate the effect of the filtering in the extrinsic mean-field variable in all the possible parameter spaces as in figure 6 but for three different (increasing) values of β and in the presence of the intrinsic filtering $\alpha = 5.0$, which actually favors both the homogeneous and heterogeneous steady states.

The dynamical states and their transitions along with the bistable regions in the two-parameter phase diagrams in figure 7 are similar to those observed in figure 6. The first, second and third column in figure 7 are plotted for increasing weak extrinsic filtering assigning $\beta = 4.0, 8.0$ and 12.0, respectively. The dynamical transitions are shown in the (ε, p) parameter space for $Q = 0.5$ in figures 7(a)–(c). It elucidates that there is a change in the stablility of the stable trivial steady state (comprising the AG) upon increasing the cut-off frequency of the extrinsic filtering resulting in an increase in the spread of the COS. Consequently, there is reviving of oscillations in the same parameter space where the oscillators suffered the AG without any oscillatory behavior. The weak extrinsic filtering does not only destabilize the stable homogeneous steady state but also destabilizes the stability of the heterogeneous symmetry breaking states in a large range of the parameter space, which corroborates that the extrinsic filtering can be a powerful tool to retain sustained oscillations among the coupled oscillators against the deterioration that renders the oscillators to inactive states loosing macroscopic oscillations. The observed dynamical states shown in figures 7(d)–(f) in the (ε, Q) parameter space for $p = 0.8$ elucidate that large values of Q favors the oscillatory state in the entire explored range of ε. Further, it is also evident that large values of β destabilize stable homogeneous and heterogeneous steady states facilitating the manifestation of the oscillatory state in a large range of the parameters. It also evident from figures 7(g)–(i) depicted for $p = 0.8$ and $Q = 0.5$ in the (ε, α) parameter space that higher values of α (weak intrinsic filtering) favor stable homogeneous and heterogeneous steady states, whereas higher values of β (weak extrinsic filtering) favor the oscillatory state by destabilizing the stable steady states thereby corroborating the counterintuitive roles of the intrinsic and extrinsic filtering on the robustness of the dynamical states.

The spread of the observed dynamical states in the (α, β) parameter space in the range of $\varepsilon \in (0, 15), p \in (0, 1)$ and $Q \in (0, 1)$ are depicted in figures 8(a)–(c), respectively. As in figure 4(b), the spread of each dynamical state as a function of a third parameter are observed for fixed α and β, which is

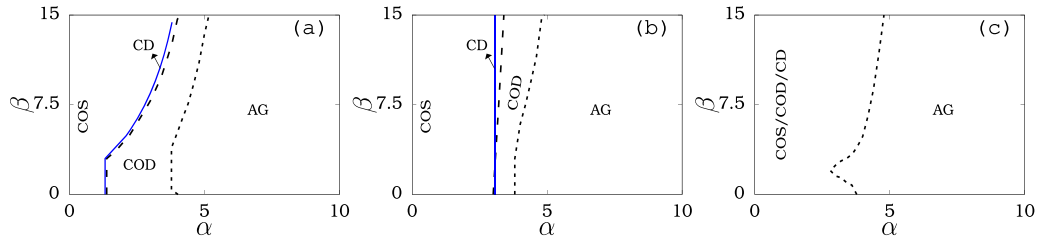

Figure 8. Global dynamical behaviors in coupled Stuart–Landau limit-cycle oscillators in (α, β) space, for (a) $p = 0.8, Q = 0.5$, $\varepsilon \in (0, 15)$, (b) $\varepsilon = 7.0, Q = 0.5, p \in (0, 1)$, and (c) $\varepsilon = 7.0, p = 0.5, Q \in (0, 1)$. This figure is illustrated to unravel the complete region of the observed dynamical states as the p, Q and ε are varied in the explored range as a function of both intrinsic and extrinsic filtering in the (α, β) parameter space. It displays the maximum possible spread of the observed dynamical states in the appropriate parameter space.

then repeated for different α to yield a set of spreads corresponding to each dynamical state. Superimposing all the set will provide a unified spread of the observed dynamical states as a function of α for the entire range of the third parameter. This procedure has to be repeated again as a function of β to obtain a global spread of the observed dynamical states in the (α, β) parameter space. Now, for any value of the third parameter, the spread of the observed dynamical states will lie only within the global spread of the COS, AG, COD, and CD regions shown in figure 8. The spread of the COS state is observed in the entire explored range of α and β in figures 8(a)–(c). CD (COD/AG) is observed as a function of α after the continuous (dashed/dotted) line in the entire range of β in figures 8(a) and (b). The COS, COD and CD states are observed in the entire explored range of α and β in figure 8(c). AG is emerges as a function of α after the dotted line in the entire range of β. It is evident from figures 8(a)–(c) that large values of β favor COS and a large α favor AG including the heterogeneous COD and CD states.

5. Summary and conclusions

We have investigated effects of the mean-field intensity, symmetry breaking coupling, as well as intrinsic and extrinsic filtering on the AG along with other observed dynamical states and their transition in an ensemble of paradigmatic Stuart–Landau limit-cycle oscillators, comprising active and inactive oscillators. For a fixed fraction of inactive oscillators, the symmetry breaking coupling facilitates the transition from the COS to the COD state via the AG. There is a finite range of spread of these dynamical states as a function of the coupling strength $Q = 1$. The spread of the AG, COD and CD states increases upon limiting the mean-field interaction by decreasing the mean-field intensity parameter Q. Further, Q is found to facilitate the onset of the homogeneous and heterogeneous states even for low values of ε. Large values of ε favors the heterogeneous states in the entire range of Q. In addition, even a weak intrinsic filtering favors the onset of the AG, while a feeble extrinsic filtering favors the oscillatory state revealing the counterintuitive roles of the intrinsic and extrinsic filtering. Similar effects are observed even when varying the proportion of the inactive oscillators p as a function of Q, ε, α and β.

In general, large values of the intrinsic cut-off frequency α favors the onset of the AG, COD and CD states even in the presence of a large proportion of inactive oscillators. In contrast, large values of the extrinsic cut-off frequency β and the mean-field intensity parameter Q favors the oscillatory state even in the presence of a large proportion of inactive oscillators and intrinsic filtering, which actually favors the stable homogeneous and heterogeneous steady states. It is to be noted that the CD state is observed for the first time in the AG literature, which manifests due to the symmetry breaking coupling. Further, the transition from the COS to the AG state occurs via an inverse HB, while the transition from AG to COD state onsets via a supercritical PB. The analytical bifurcation curves have also been deduced and found to agree very well with the numerical boundaries. These results corroborate that extrinsic filtering and the mean-field intensity parameter can be used as a powerful tool to retain self-sustained oscillations among the coupled oscillators against the deterioration that renders the oscillators to inactive states loosing macroscopic dynamical states. Our study also revealed that such collective dynamics can be engineered as desired by using the filtering in the extrinsic and intrinsic variable thereby generalizing the studies on the AG and means to control the AG to preserve macroscopic activity.

Acknowledgments

KS thank the DST-SERB, Government of India, for providing National Post Doctoral fellowship under the Grant No. PDF/2019/001589. DVS is supported by the CSIR EMR Grant No. 03(1400)/17/EMR-II. The

work of VKC forms part of a research project sponsored by CSIR Project under Grant No. 03(1444)/18/EMR-II. WZ acknowledges support from Research Starting grants from South China Normal University (8S0340) and a project supported by Guangdong Province Universitties and Colleges Pearl River Scholar Funded Scheme (2018). JK was supported by the project RF Goverment Grant 075-15-2019-1885.

ORCID iDs

D V Senthilkumar https://orcid.org/0000-0003-1902-972X

References

[1] Pikovsky A, Rosenblum M and Kurths J 2001 *Synchronization: A Universal Concept in Nonlinear Sciences* (Cambridge: Cambridge University Press)
[2] Boccaletti S, Kurths J, Osipov G, Valladares D L and Zhou C S 2002 *Phys. Rep.* **366** 1
[3] Boccaletti S, Latora V, Moreno Y, Chavez M and Hwang D U 2006 *Phys. Rep.* **424** 175
[4] Arenas A, Díaz-Guilera A, Kurths J, Moreno Y and Zhou C S 2008 *Phys. Rep.* **469** 93
[5] Lakshmanan M and Senthilkumar D V 2011 *Dynamics of Nonlinear Time-Delay Systems* (Berlin: Springer)
[6] Saxena G, Prasad A and Ramaswamy R 2012 *Phys. Rep.* **521** 205
[7] Koseska A, Volkov E and Kurths J 2013 *Phys. Rep.* **531** 173
[8] Koseska A, Volkov E and Kurths J 2013 *Phys. Rev. Lett.* **111** 024103
[9] Zakharova A, Kapeller M and Schöll E 2014 *Phys. Rev. Lett.* **112** 154101
[10] Koseska A, Ullner E, Volkov E I, Kurths J and Ojalvo J G 2010 *J. Theor. Biol.* **263** 189202
[11] Yao N and Zheng Z 2016 *Int. J. Mod. Phys.* B **30** 1630002
[12] Schöll E 2016 *Eur. Phys. J. Spec. Top.* **225** 891
[13] Panaggio M J and Abrams D M 2015 *Nonlinearity* **28** R67–87
[14] Winfree A T 2001 *The Geometry of Biological Time* (New York: Springer)
[15] Pfurtscheller G and Neuper C 1994 *Neurosci. Lett. Suppl.* **174** 93
[16] Krause C M, Lang A H, Laine M, Kuusisto M and Pörn B 1996 *Electroencephalogr. Clin. Neurophysiol.* **98** 319
[17] Leocani L, Toro C, Manganotti P, Zhuang P and Hallet M 1997 *Electroencephalogr. Clin. Neurophysiol.* **104** 199
[18] Pfurtscheller G and Lopes da Silva F H 1999 *Clin. Neurophysiol.* **110** 1842
[19] Daido H and Nakanishi K 2004 *Phys. Rev. Lett.* **93** 104101
[20] Pahwa S, Scoglio C and Scala A 2015 *Sci. Rep.* **4** 3694
[21] Daido H and Nakanishi K 2007 *Phys. Rev.* E **75** 056206
[22] Daido H 2009 *Europhys. Lett.* **87** 40001
Daido H 2011 *Phys. Rev.* E **83** 026209
[23] Huang W, Zhang X, Hu X, Zou Y, Liu Z and Guan S 2014 *Chaos* **24** 023122
[24] Tanaka G, Morino K, Daido H and Aihara K 2014 *Phys. Rev.* E **89** 052906
[25] Daido H 2008 *Europhys. Lett.* **84** 10002
[26] Morino K, Tanaka G and Aihara K 2011 *Phys. Rev.* E **83** 056208
[27] Thakur B, Sharma D and Sen A 2014 *Phys. Rev.* E **90** 042904
[28] Kundu S, Majhi S, Karmakar P, Ghosh D and Rakshit B 2018 *Europhys. Lett.* **123** 30001
[29] Kundu S, Majhi S and Ghosh D 2018 *Phys. Rev.* E **97** 052313
[30] Sun S, Ma N and Xu W 2017 *Sci. Rep.* **7** 42715
[31] Liu Y, Zou W, Zhan M, Duan J and Kurths J 2016 *Europhys. Lett.* **114** 40004
[32] Gowthaman I, Sathiyadevi K, Chandrasekar V K and Senthilkumar D V 2020 *Nonlinear Dyn.* **100** xxxxx
[33] Sathiyadevi K, Gowthaman I, Senthilkumar D V and Chandrasekar V K 2019 *Chaos* **29** 123117
[34] Ponrasu K, Gowthaman I, Chandrasekar V K and Senthilkumar D V 2019 *Europhys. Lett.* **128** 58033
[35] Ray A, Kundu S and Ghosh D 2019 *Europhys. Lett.* **128** 40002
[36] Kundu S, Majhi S, Sasmal S K, Ghosh D and Rakshit B 2017 *Phys. Rev.* E **96** 062212
[37] Banerjee T and Ghosh D 2014 *Phys. Rev.* E **89** 052912
[38] Ghosh D, Banerjee T and Kurths J 2015 *Phys. Rev.* E **92** 052908
[39] Banerjee T, Biswas D, Ghosh D, Schöll E and Zakharova A 2018 *Chaos* **28** 113124
[40] Zou W, Ocampo-Espindola J L, Senthilkumar D V, Kiss I Z, Zhan M and Kurths J 2019 *Phys. Rev.* E **99** 032214
[41] Kumar K, Biswas D, Banerjee T, Zou W, Kurths J and Senthilkumar D V 2019 *Phys. Rev.* E **100** 052212
[42] Pyragas K, Pyragas V, Kiss I Z and Hudson J L 2002 *Phys. Rev. Lett.* **89** 244103
[43] Schmidt L and Krischer K 2015 *Phys. Rev. Lett.* **114** 034101
[44] Chandrasekar V K, Gopal R, Senthilkumar D V and Lakshmanan M 2016 *Phys. Rev.* E **94** 012208
[45] Abrams D M and Strogatz S H 2004 *Phys. Rev. Lett.* **93** 174102
[46] Premalatha K, Chandrasekar V K, Senthilvelan M and Lakshmanan M 2015 *Phys. Rev.* E **1** 052915
[47] Premalatha K, Chandrasekar V K, Senthilvelan M and Lakshmanan M 2016 *Phys. Rev.* E **93** 052213
[48] Sathiyadevi K, Chandrasekar V K, Senthilkumar D V and Lakshmanan M 2018 *Phys. Rev.* E **97** 032207
[49] Schneider I, Kapeller M, Loos S, Zakharova A, Fiedler B and Schöll E 2015 *Phys. Rev.* E **92** 052915
[50] Sathiyadevi K, Chandrasekar V K and Senthilkumar D V 2018 *Phys. Rev.* E **98** 032301
[51] Aoyagi T 1995 *Phys. Rev. Lett.* **74** 4075
[52] Tukhlina N and Rosenblum M 2008 *J. Biol. Phys.* **34** 301
[53] Izhikevich E M 2007 *Dynamical Systems in Neuroscience: The Geometry of Excitability and Bursting* (Cambridge, MA: MIT Press)
[54] Banerjee T, Dutta P S and Gupta A 2015 *Phys. Rev.* E **91** 052919
[55] Garcia-Ojalvo J, Elowitz M B and Strogatz S H 2004 *Proc. Natl Acad. Sci. USA* **101** 10955
[56] Ullner E, Zaikin A, Volkov E I and Garcia-Ojalvo J 2007 *Phys. Rev. Lett.* **99** 148103
[57] Ullner E, Koseska A, Kurths J, Volkov E, Kantz H and Garcia-Ojalvo J 2008 *Phys. Rev.* E **78** 031904